Matrix Metalloproteinase 10 Degradomics in Keratinocytes and Epidermal Tissue Identifies Bioactive Substrates With Pleiotropic Functions*[S]

Pascal Schlage‡, Tobias Kockmann‡, Fabio Sabino‡, Jayachandran N. Kizhakkedathu§, and Ulrich auf dem Keller‡¶

Matrix metalloproteinases (MMPs) are important players in skin homeostasis, wound repair, and in the pathogenesis of skin cancer. It is now well established that most of their functions are related to processing of bioactive proteins rather than components of the extracellular matrix (ECM). MMP10 is highly expressed in keratinocytes at the wound edge and at the invasive front of tumors, but hardly any non-ECM substrates have been identified and its function in tissue repair and carcinogenesis is unclear. To better understand the role of MMP10 in the epidermis, we employed multiplexed iTRAQ-based Terminal Amine Isotopic Labeling of Substrates (TAILS) and monitored MMP10-dependent proteolysis over time in secretomes from keratinocytes. Time-resolved abundance clustering of neo-N termini classified MMP10-dependent cleavage events by efficiency and refined the MMP10 cleavage site specificity by revealing a so far unknown preference for glutamate in the P1 position. Moreover, we identified and validated the integrin alpha 6 subunit, cysteine-rich angiogenic inducer 61 and dermokine as novel direct MMP10 substrates and provide evidence for MMP10-dependent but indirect processing of phosphatidylethanolamine-binding protein 1. Finally, we sampled the epidermal proteome and degradome in unprecedented depth and confirmed MMP10-dependent processing of dermokine *in vivo* by TAILS analysis of epidermis from transgenic mice that overexpress a constitutively active mutant of MMP10 in basal keratinocytes. The newly identified substrates are involved in cell adhesion, migration, proliferation, and/or differentiation, indicating a contribution of MMP10 to local modulation of these processes during wound healing and cancer development. Data are available via ProteomeXchange with identifier PXD002474. ***Molecular & Cellular Proteomics 14: 10.1074/mcp.M115.053520, 3234–3246, 2015.***

Matrix metalloproteinases (MMPs)[1] are extracellular zinc-dependent endoproteinases that are highly expressed in tissues undergoing remodeling processes during development, in response to injury, or as a result of neoplastic transformation (1–3). MMP10, also known as stromelysin-2, gained particular interest in the skin, because of its specific and strong expression in wound edge keratinocytes as well as at the invasive front of epithelial tumors (4–6). Overexpression of a constitutively active MMP10 mutant in wound keratinocytes in mice led to scattering of these cells at the tip of the migrating wound epithelium, altered β1-integrin expression, reduced AKT phosphorylation and increased apoptosis (7). Lack of MMP10 in a lung infection model affected genes that are involved in the regulation of apoptosis, cell proliferation, immune response and signal transduction (8). In the gut, bone marrow-derived MMP10 had a protective role in experimental colitis with implications in macrophage polarization (9). MMP10 released from hepatocytes and macrophages positively contributed to liver regeneration (10), whereby it promoted hepatocarcinogenesis in a complicated crosstalk with chemokine signaling (11). Most recently, Rohani *et al.* dem-

From the ‡ETH Zurich, Department of Biology,Institute of Molecular Health Sciences, Otto-Stern-Weg 7, 8093 Zurich, Switzerland; §University of British Columbia, Department of Pathology and Laboratory Medicine and Department of Chemistry, Centre for Blood Research, 4.401Life Sciences Institute, 2350 Health Sciences Mall, Vancouver, British Columbia, Canada V6T 1Z3

Received July 9, 2015, and in revised form, October 16, 2015
Published, MCP Papers in Press, October 16, 2015, DOI 10.1074/mcp.M115.053520
Author contributions: U.a.d.K. designed research; P.S., T.K., and F.S. performed research; J.N.K. contributed new reagents or analytic tools; P.S. and U.a.d.K. analyzed data; P.S. and U.a.d.K. wrote the paper.

[1] The abbreviations used are: MMP, matrix metalloproteinase; iTRAQ™, isobaric tag for relative and absolute quantitation; TAILS, terminal amine isotopic labeling of substrates; ECM, extracellular matrix; TIMP, tissue inhibitor of metalloproteinase; ITGA6, integrin alpha 6 subunit; CYR61, cysteine-rich angiogenic inducer 61; DMKN, dermokine; PEBP1, phosphatidylethanolamine-binding protein 1; MMRRC, mutant mouse regional resource center; MPK, mouse primary keratinocyte; HPG-ALD, hyperbranched polyglycerol aldehydes; NCE, normalized collision energy; HCD, higher-energy collisional dissociation; TPP, trans-proteomic pipeline; ITGB4, integrin beta 4 subunit; SDC4, syndecan-4; ERK: extracellular-signal regulated kinase; RKIP, Raf kinase inhibitory protein; HCNP, hippocampal cholinergic neurostimulating peptide.

onstrated a role for macrophage-derived MMP10 in moderating scar formation by controlling collagenase activity of dermal macrophages (12).

Similar complex phenotypes have been associated with activities of most MMPs that, however, were not related to processing of extracellular matrix (ECM) proteins, the classical MMP substrates (13), but of bioactive mediators, including cell surface receptors, growth factor binding proteins, proteases, inhibitors, cytokines, and chemokines (14, 15). This changed the view on MMPs as simple tissue degraders to precise modulators of diverse processes, such as cell proliferation, migration, differentiation, angiogenesis, apoptosis and immune response (2, 16). As an example, functions of MMP3, the closest homolog of MMP10, in keratinocyte differentiation (17), tumor cell invasion (18), and immune cell recruitment (19) could be explained by processing of non-ECM proteins that have been identified as direct substrates of this protease (2, 20) in addition to ECM components (21). However, because MMP10 has been mostly neglected in the quest for new MMP substrates, it remains to be elucidated, if it also exerts its functions in part by processing of bioactive proteins whose identification is instrumental in understanding the mechanisms of action of MMP10 in tissue repair and carcinogenesis.

Recently, we applied iTRAQ-based Terminal Amine Isotopic Labeling of Substrates (TAILS), a multiplexed quantitative proteomics workflow for identification of protease substrates in complex proteomes (22–24), to reveal new targets of MMP10 in secretomes from mouse embryonic fibroblasts (25). Moreover, to mimic MMP10 activity at the epidermal–dermal interface, we devised a new workflow that allowed monitoring both cellular origins and cleavages of substrates in mixed secretomes from keratinocytes and fibroblasts (26). However, this study focused on basement membrane components and missed additional information on cleavage kinetics. Thus, in this work, we employed time-resolved TAILS to identify novel MMP10 substrates in keratinocyte secretomes and mouse epidermal tissue, aiming at further characterizing the MMP10 substrate degradome in epidermal keratinocytes for a better understanding of its biological roles in the skin. Here, we identified novel bioactive substrates of MMP 10 *in vitro* and in the skin *in vivo*, which provide insight into its functions in wound repair and carcinogenesis. In addition, we revealed an unexpected preference of MMP10 for substrates that harbor a glutamate residue in P1 position, which might be exploited for the development of specific activity-based probes or inhibitors for this important wound- and tumor-related protease.

EXPERIMENTAL PROCEDURES

Cell Growth and Preparation of Secreted Proteins—MMP10 knockout mice were obtained from the Mutant Mouse Regional Resource Center (MMRRC) at UC Davis (strain# 011737-UCD). Mouse primary keratinocytes (MPKs) were isolated and immortalized as described previously (27, 28). Immortalized MPKs were grown in Defined K-SFM (Life Technologies, Zug, Switzerland) supplemented with 1% penicillin/streptomycin, 0.1 mM cholera toxin and 10 ng/ml epidermal growth factor. Secreted proteins were collected as described (26). Briefly, MPKs were washed three times with PBS and incubated with serum-free EpiLife medium (phenol red free, Life Technologies) supplemented with 60 μM $CaCl_2$ for 24 h. Afterward, supernatants were collected, 0.5 mM PMSF was added, and cell debris was removed by centrifugation at 4000 rpm and 4 °C for 30 min. Supernatants were filtered (0.22 μm pore size), concentrated by ultrafiltration, followed by buffer exchange to 50 mM HEPES (pH 7.8) using Amicon Ultra-15 centrifugal filter units (3 kDa cut-off, Millipore, Billerica, MA). Protein concentration was determined by Bradford assay (BioRad, Hercules, CA), and adjusted secretomes (2 mg/ml in 50 mM HEPES (pH 7.8)) were stored at −80 °C until further use.

MMP10 Auto-activation and Incubation of Secretomes—Recombinant human MMP10 (910-MP-010; R&D Systems, Minneapolis, MN) was auto-activated by fivefold dilution in 50 mM HEPES (pH 7.8) and incubation for 16 h at 37 °C. Secretomes of MMP10-deficient keratinocytes were incubated with active MMP10 at an enzyme/protein ratio of 1:170 (w/w) in the presence of 10 mM $CaCl_2$ and 100 mM NaCl for up to 16 h at 37 °C. Samples for controls at 0 and 16 h were incubated with an equivalent volume of buffer without MMP10.

Preparation of Epidermal Lysates from Mouse Skin—Eight-week-old female mice (hemizygous K14-MMP10 or wild-type animals) (7) were euthanized by CO_2 inhalation, and the back of the animals was shaved before isolation of full skin samples. To separate epidermis from dermis by heat shock, full skin biopsies were incubated in PBS pre-warmed to 60 °C for 1 min, followed by 4 °C PBS for 30 s. Epidermis was scraped off with a scalpel in T-PER solution (Pierce, Rockford, IL) supplemented with protease inhibitor mixture tablet (cOmplete, Roche, Mannheim, Germany) and transferred to a round bottom tube. Samples were homogenized in a total volume of 2 ml T-PER solution using an Ultra-Turrax dispersing instrument (Janke & Kunkel, Staufen, Germany). After centrifugation at 13,000 rpm for 15 min at 4 °C the intermediate phase was transferred to new tubes and frozen. For 4plex-iTRAQ-TAILS analysis proteins were precipitated by addition of six volumes of ice-cold acetone (4 h at −20 °C), pelleted by centrifugation (13,000 rpm, 30 min, 4 °C) and resuspended at a concentration of 1 mg/ml in TAILS buffer (2.5 M GuHCl, 250 mM HEPES, pH 7.8).

8plex-iTRAQ-TAILS (Keratinocyte Secretomes) and 4plex-iTRAQ-TAILS (Epidermal Lysates) Protocols—iTRAQ-TAILS procedure followed the previously published protocol (23) using 4plex-iTRAQ reagents, or 8plex-iTRAQ reagents as already described (25). Briefly, aliquots of 0.25 mg of MMP10-treated or control keratinocyte secretomes (8plex), or aliquots of 0.5 mg of epidermal lysates of K14-MMP10 or wild-type mice (4plex) were labeled on the protein level with iTRAQ reagents at a 1:4 protein/iTRAQ (w/w) ratio. Labeled proteins were tryptic digested (Trypsin Gold, Promega, Madison, WI; 1:100 enzyme/protein (w/w)), and 10% of the resulting peptide mixture was removed for analysis before enrichment of N-terminal peptides. The remaining peptide mixture was enriched for N-terminal peptides by incubation with threefold excess (w/w) of 435 kDa HPG-ALD polymer (available without commercial or company restriction from Flintbox Innovation Network, The Global Intellectual Exchange and Innovation Network (http://www.flintbox.com/public/project/1948/)) and subsequent ultrafiltration using Amicon Ultra-0.5 centrifugal filter units (5 kDa cut-off, Millipore). HPG-ALD polymers consist of a hyperbranched polyglycerol backbone that has been functionalized with aldehyde groups to covalently bind internal tryptic and C-terminal peptides through their free terminal amine groups, whereas blocked N-terminal peptides are unreactive and thus specifically recovered in the flow-through upon ultrafiltration (29). Peptide mixtures were frozen and stored at −20 °C until further use.

Peptide Fractionation and LC-MS/MS Analysis—Peptide mixtures from both prior and after enrichment for protein N termini were fractionated by strong cation exchange chromatography following the previously described protocol (25). Pooled peptide fractions were either analyzed on (1) an LTQ-Orbitrap Velos mass spectrometer (Thermo Fischer Scientific, Bremen, Germany) coupled to an Eksigent-Nano-HPLC system (Eksigent Technologies, Dublin, CA) (8plex-iTRAQ-TAILS: 8plex) or on (2) a hybrid Quadrupole-Orbitrap mass spectrometer (Q Exactive, Thermo Fischer Scientific) coupled to an ultrahigh-pressure nano-LC system (Easy-nLC 1000, Thermo Fischer Scientific) combined with an ESI nanospray source (Digital PicoView, New Objective, Woburn, MA) (4plex-iTRAQ-TAILS: 4plex). Peptides were loaded onto a self-made tip column (75 μm $\times$ 150 mm) packed with C18 material (AQ, 3 μm 200 Å, Bischoff GmbH, Leonberg, Germany) and separated at a flow rate of 250 nL/min with a linear gradient from 8 to 30% of Buffer B within 60 min (8plex) or at a flow rate of 300 nL/min with a linear gradient from 2 to 37% Buffer B within 120 min (4plex). Buffer A: aqueous 0.1% formic acid. Buffer B: 100% MeCN, 0.1% formic acid. Full scan MS spectra (8plex: 300–1700 *m/z*; 4plex: 400–2000 *m/z*) were acquired with a resolution of 30 k (8plex) or 70 k (4plex) after accumulation to a target value of 1E6. 8plex: Collision induced dissociation (CID) MS/MS spectra were recorded in a data-dependent manner in the ion trap from the eight most intense signals using a normalized collision energy (NCE) of 35% with an activation time of 10 ms. For the detection of iTRAQ reporter ions, the same precursors were selected again for fragmentation using higher-energy collisional dissociation (HCD) with a NCE of 45%, and the spectra were recorded at a resolution of 7500 at 400 m/z. 4plex: HCD MS/MS spectra with fixed first mass 100 m/z for the 15 most abundant precursor ions were recorded at a resolution of 17.5 k applying an automatic gain control target value of 2E5 and a maximum injection time of 120 ms. Precursors were isolated using a window of 2 *m/z* and fragmented at 30% NCE. The underfill ratio of the orbitrap mass analyzer was set to 5%, and precursor ions below the intensity threshold of 8.3E4 were excluded from fragmentation. Precursor ions (4plex and 8plex) with unassigned or single charge states were rejected, and precursor masses already selected for MS/MS were excluded for further selection for 10 s (8plex) or 45 s (4plex).

MS Data Analysis—Mascot Distiller v2.4.3.3 (Matrix Science, Boston, MA) was used to extract peak lists from raw files and for merging of corresponding CID/HCD spectra pairs (8plex). Peak lists (mgf) were searched by Mascot v2.4.1 search engine against a mouse UniProtKB database (release 2014_03; 50807 entries), to which sequences for human MMP10, reversed decoys and common contaminants had been added and with following parameters: semi-Arg-C for enzyme specificity allowing up to 1 missed cleavage; carbamidomethyl(C), iTRAQ(K) as fixed modifications; acetyl(N-term), iTRAQ(N-term), pyroQ(N-term), and oxidation(M) as variable modifications; parent mass error at 10 ppm, fragment mass error at 0.8 Da (Q Exactive: 0.02 Da). The Trans-Proteomic Pipeline (TPP v4.8, rev 0, Build 201501131705) (30) was used to secondary validate Mascot search results and to compile a single peptide list from all peptide fractions obtained from both samples (with and without N-terminal enrichment). First, data were processed by PeptideProphet setting the "minimum peptide length" to 7, applying "accurate mass binning (PPM)," omitting the "NTT model," "leaving alone all entries with asterisked score values" (4plex only), and using "decoy hits to pin down the negative distribution." Next, iProphet was employed for additional validation, and only peptides with an iProphet probability of $\geq$ 0.9 (corresponding to an error rate of $<$ 1%) were included in subsequent analyses. For relative quantification iTRAQ reporter ion intensities were extracted from mgf files using a modified version of i-Tracker (25, 31) with a mass tolerance of 0.1 Da and purity corrections supplied by the iTRAQ manufacturer and assigned to filtered peptides.

Peptide/Protein Quantification, Annotation, Clustering, Generation of Sequence Logos and Secondary Structure Analysis—Multiple CIDs were merged, and peptides were assigned to proteins and annotated for their position in the processed mature protein using the CLIPPER analysis pipeline (32). For time-resolved analysis (8plex) iTRAQ reporter ion intensities were normalized to the sum of all channels and a maximum of 1.0 for the highest value, and abundance clustering was performed using the Mfuzz package for R (version 2.15.3; http://www.r-project.org/) (33) and the mestimate() function to determine optimal fuzzication parameters (34). Prism 5.0 (GraphPad Software) was used for curve fitting. Cleavage site specificities were calculated by WebPICS (35), and logos were generated using IceLogo (36). Protein and peptide quantification in epidermal lysates (4plex) was performed as described (37) and $\log_2$-ratios calculated from iTRAQ reporter ion intensities upon quantile normalization. Statistical tests for differential abundance of proteins and peptides were performed with MeV v4.8 (38). Secondary structures were predicted using a local installation of psipred version 3.5 (39) and visualized with WebLogo version 3.3 (40).

MMP10 Activity Assay—Synthetic peptide substrates containing an N-terminal fluorescent 7-methoxycoumarinyl-4-acetyl (Mca) group that is quenched by a C-terminal 2,4-dinitrophenyl (Dnp) group with sequences Mca-PAA $\downarrow$ LVA-Lys(Dnp)-NH_2, Mca-PAE $\downarrow$ LVA-Lys-(Dnp)-NH_2 and Mca-PAN $\downarrow$ LVA-Lys(Dnp)-NH_2 were obtained from JPT Peptide Technologies (Berlin, Germany). The scissile bond is indicated by an arrow in the sequence. Enzyme activity of auto-activated MMP10 (final concentration 19 nM) buffered in 50 mM Tris-HCl (pH 7.5), 10 mM $CaCl_2$, 150 mM NaCl, 0.05% (w/v) Brij-35 was monitored by reading fluorescence (excitation 320 nm, emission 405 nm) in kinetic mode in the presence of 10 μM peptide substrate at 37 °C with a SpectraMax Gemini XS spectrofluorometer (Molecular Devices, Sunnyvale, CA). Methoxycoumarinyl-4-acetic acid (Mca-OH) was used as calibration standard for the determination of k_{cat}/K_m values, and data were analyzed with SoftMax Pro (version 4.3.1).

Substrate Docking—The hexapeptide (PAE $\downarrow$ LVA) representing the cleavage site of the most efficient peptide substrate was docked into the active site cleft of MMP10 using the crystal structure of the catalytic domain of human MMP10 (PDB 1q3a) (41). Energy minimization based on flexible ligand docking, modeling and images were generated with the UCSF Chimera package using DOCK6 (42) from the Resource for Biocomputing, Visualization and Informatics at the University of California, San Francisco.

Substrate Cleavage Assays—Recombinant human CYR61 (120–25; Peprotech, Rocky Hill, NJ), integrin alpha-6/beta-4 (5497-A6; R&D Systems), DMKN (TP325655; OriGene, Rockville, MD) or PEBP1 (PRO-722; Prospec, East Brunswick, NJ) were incubated with active recombinant human MMP10 (auto-activated), MMP2 (902-MP-010; R&D Systems) or MMP9 (kind gift from Chris Overall (UBC Vancouver)) (both activated by 4-aminophenylmercuric acetate (APMA) (1 mM; 1 h)) at a molecular enzyme/substrate ratio of 1:10 in 50 mM Tris-HCl (pH 7.5), 200 mM NaCl and 5 mM $CaCl_2$ for 16 h at 37 °C. Reaction products were visualized by SDS-PAGE followed by silver staining or immunoblot analysis.

Immunoblot Analysis—Concentrated secretomes from MMP10 knockout keratinocytes or recombinant proteins incubated with auto-activated recombinant MMP10 were subjected to SDS-PAGE, transferred to nitrocellulose membranes and probed with primary antibodies raised against ITGA6 (HPA012696; Sigma-Aldrich, Buchs, Switzerland), CYR61 (HPA029853; Sigma), DMKN (16252–1-AP; Proteintech, Chicago, IL) or PEBP1 (HPA008819; Sigma). Bands were visualized by enhanced chemiluminescence reaction using horserad-

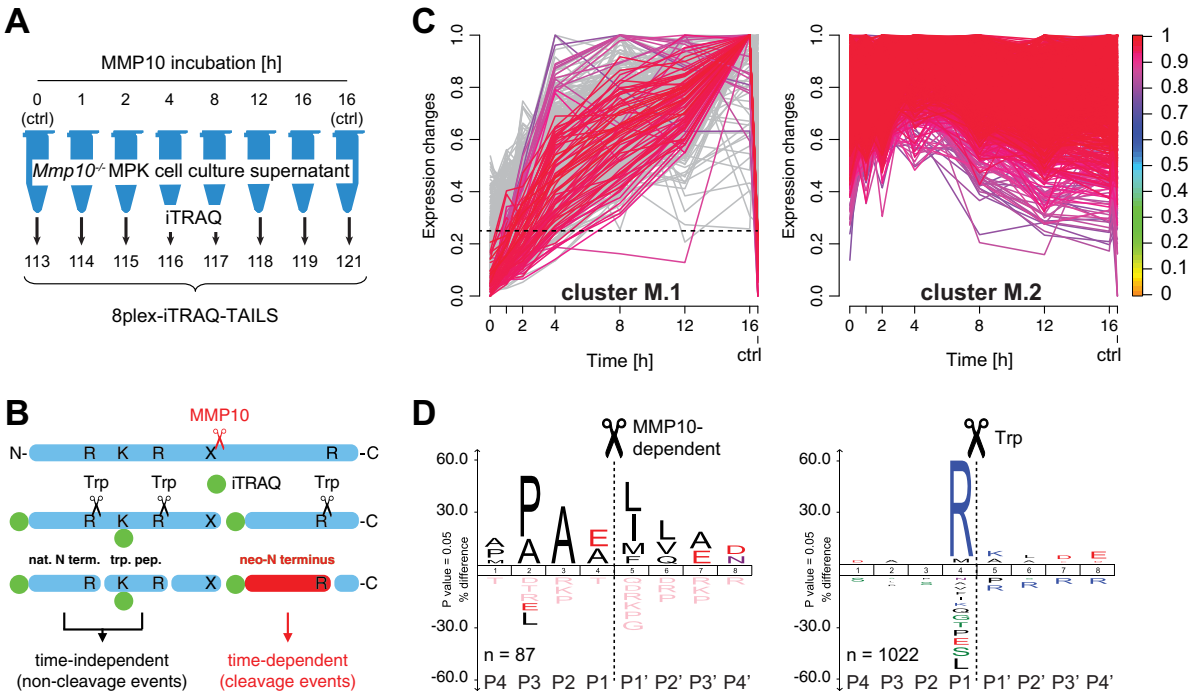

FIG. 1. **MMP10 substrate discovery in keratinocyte secretomes.** *A*, Experimental setup. Secretomes from MMP10 knockout mouse primary keratinocytes (MPK) were incubated with recombinant MMP10 for increasing periods of time and analyzed by 8plex-iTRAQ-TAILS. Controls (ctrl) were incubated in buffer without MMP10 for 0 and 16 h, respectively. *B*, Time-dependent generation of neo-N termini (cleavage events) by MMP10 and time-independent release of internal tryptic peptides (trp. pep.) and natural N termini (nat. N term.) by trypsin (Trp) during iTRAQ-TAILS analysis. *C*, Fuzzy c means clustering of abundance profiles of neo-N termini, quantifiable internal tryptic peptides and natural N termini. Peptides with a time-dependent increase in abundance after MMP10 incubation (cluster M.1) are separated from peptides with a relatively constant abundance over time (cluster M.2). Colorkey indicates membership value α. Dashed line defines cut-off (0.25) for relative abundance levels in control channels (0 and ctrl) for MMP10-dependent events. *D*, IceLogo analysis of cleavage sites corresponding to peptides in cluster M.1 and cluster M.2. High prevalence of P in P3 and/or L/I in P1′ positions for cleavages in cluster M.1 (neo-N termini; time-dependent) indicate MMP cleavage specificity. Peptides assigned to cluster M.2 (time-independent) are dominated by internal tryptic peptides (R in P1) or natural N termini (*e.g.* M in P1; initiator methionine removed).

ish peroxidase conjugated secondary antibodies and x-ray films (Fuji Medical, Tokyo, Japan).

Zymography—Gelatin zymography was performed using SDS-PAGE containing 1 mg/ml gelatin as previously described (25). To visualize proMMP9 activation by MMP10, recombinant human proMMP9 was incubated with auto-activated MMP10 and gelatinolytic activity assessed by gelatin zymography.

The mass spectrometry proteomics data have been deposited to the ProteomeXchange Consortium (43) via the PRIDE partner repository with the dataset identifier PXD002474. MS/MS spectra for N-terminal peptides are supplied as Supplemental Data.

RESULTS

Experimental Setup and Classification of MMP10-dependent Cleavages—To characterize the MMP10 substrate degradome in epidermal keratinocytes, we incubated cell culture supernatants from MMP10-deficient mouse primary keratinocytes with recombinant human MMP10 for 1, 2, 4, 8, 12, and 16 h or buffer alone (0 and 16 h controls) and subjected them to 8plex-iTRAQ-TAILS analysis (Fig. 1*A*). By integrating data from sample analysis before and after N-terminal enrichment, we identified a total of 3454 peptides (semi-tryptic N-terminal or fully tryptic internal peptides) corresponding to 1221 proteins (supplemental Table S1). To discriminate between non-cleavage (natural N termini and tryptic internal peptides) and MMP10-dependent cleavage events (neo-N termini) (Fig. 1*B*) based on time-dependent peptide abundances in all eight conditions, we extracted 1961 iTRAQ-labeled peptides (supplemental Table S2) and applied fuzzy c means clustering, which allows identification of cleavage events with high confidence (25). Thereby, we assigned the quantifiable peptides to two clusters of cleavage (cluster M.1) and non-cleavage (cluster M.2) events using a classifier cut-off for the cluster membership value α of 0.8 and identified a total of 525 protease-generated neo-N termini with increased abundance over time (cluster M.1) (Fig. 1*C*). Next, we filtered the cluster of cleavage events for MMP10-dependent cleavages by extracting neo-N-terminal peptides whose abundance in both control channels was less than 25% of the highest abundance at any time point. Applying this filter, we extracted 87 MMP10-generated neo-N termini from cluster M.1 whose associated cleavage specificity logo showed characteristics of MMP specificity, whereas N termini related to non-cleavage events (cluster M.2) were dominated by internal tryptic peptides (Fig. 1*D*).

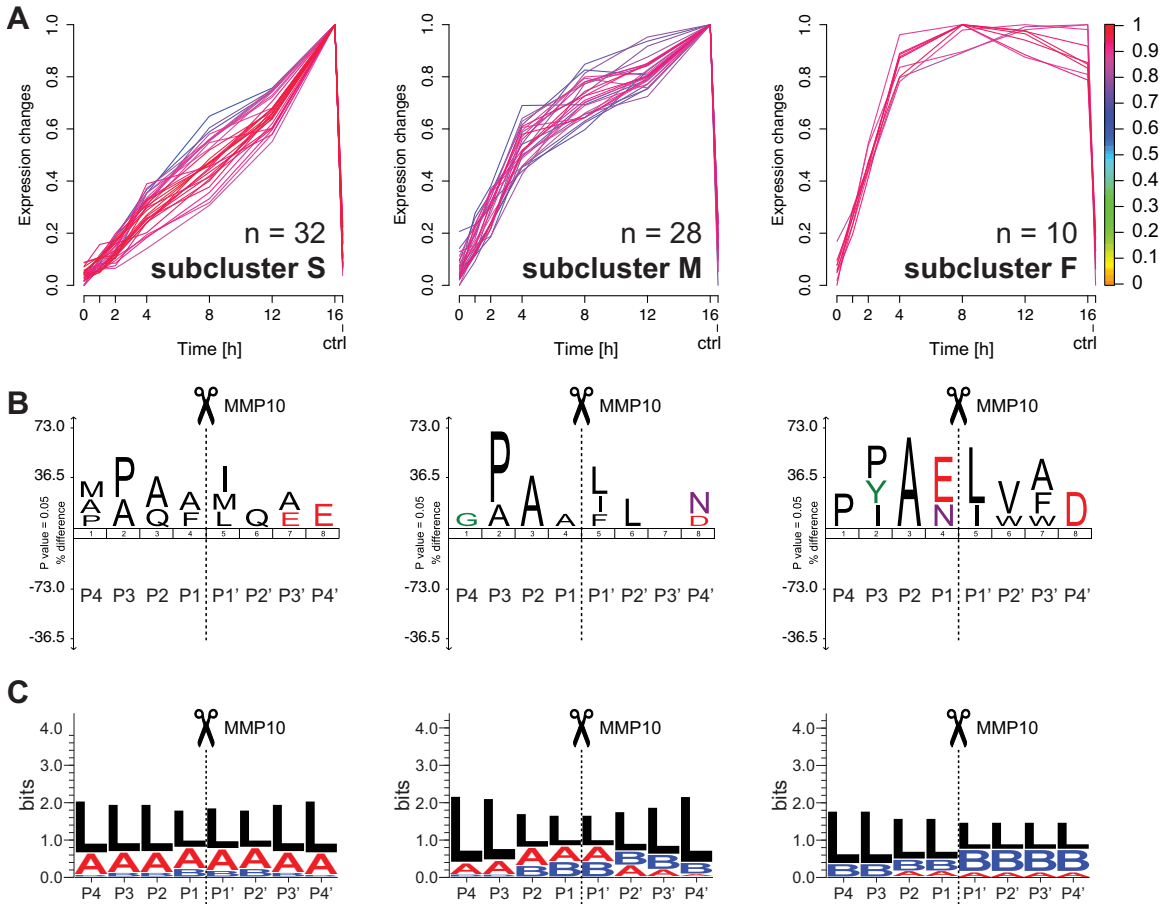

FIG. 2. **Kinetic subclassification of MMP10-dependent cleavage events.** *A*, Fuzzy c means clustering of abundance profiles of peptides in cluster M.1. Seventy peptides were assigned with a membership value of 0.7 to subclusters showing constant slow (S), medium (M), or fast (F) increase in abundance over time. Colorkey indicates membership value α. *B*, IceLogo analysis of cleavage sites corresponding to peptides assigned to each subcluster. All subclusters show high prevalence of P in P3 and/or L/I in P1′ representing classic MMP cleavage specificity. Increased prevalence of E and N in P1 in subcluster F indicates a kinetic preference of MMP10 for cleavage sites with these amino acids in the P1 position. *C*, Predicted secondary structures around scissile bonds inferred from neo-N-terminal peptides in each subcluster. Cleavages in all subclusters are primarily located in extended loops. L: loop; A: helix; B: sheet.

To further subclassify MMP10-dependent cleavages, we assigned 70 (69 unique cleavage events) of all 87 MMP10-generated neo-N termini to three subclusters based on catalytic efficiency of proteolytic processing with a cluster membership value α cut-off of 0.7 (Fig. 2*A*; supplemental Table S3). Thereby, peptides were assigned to subclusters showing a slow (subcluster S, 32 peptides), medium (subcluster M, 28 peptides) or fast (subcluster F, 10 peptides) increase in abundance over time. Analysis of cleavage specificities for each subcluster showed classical MMP specificity with P in P3 and/or I/L in P1′ for all subclusters (Fig. 2*B*). In addition, frequencies of E and N in P1 were increased in subcluster F comprising the most efficient substrate cleavage events. Importantly, this effect was not significantly influenced by structural accessibility of cleavage sites as indicated by secondary structure predictions that showed the same preference for cleavages in loops for events assigned to all three subclusters (Fig. 2*C*).

Preference of MMP10 for Substrates Harboring E in P1—The TAILS data suggested a positive influence on cleavage efficiency for MMP10 substrates that harbor an E or N in P1. To further study the influence of P1 on MMP10 cleavage efficiency, we designed fluorogenic peptide substrates based on the observed predominant specificity covering positions P3 to P3′ of subcluster F with variable amino acid residues at the P1 position (*i.e.* PAX ↓ LVA; X = A, E or N). Indeed, activity assays with recombinant MMP10 demonstrated that the peptide with E in P1 was most efficiently cleaved with a k_{cat}/K_m value of 4471 M-1 s-1, whereas the peptide with A in P1 was processed much slower with a k_{cat}/K_m value of 183 M-1 s-1. Interestingly, the peptide with N in P1 was not cleaved under the tested conditions (Fig. 3*A*), indicating additional influences other than the primary cleavage sequence such as noncatalytic substrate binding on efficiency of processing of protein substrates. To find a possible explanation for the kinetic preference for E in P1, we next used the hexapeptide sequence

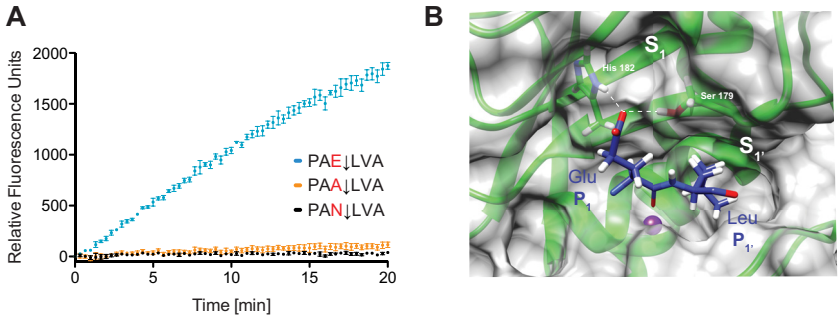

FIG. 3. **Influence of P1 on cleavage efficiency.** *A*, MMP10 activity assay using fluorogenic peptides harboring either A, N, or E in P1 and recombinant MMP10. MMP10 processed the peptide substrate with E in P1 with much higher efficiency than the other hexapeptides. Measurements were performed in triplicates; error bars represent standard deviation of the mean. *B*, Structural model depicting possible interactions via hydrogen-bond formation between the carboxyl side chain of E in P1 and His^{182} and Ser^{179} of the S1′ pocket of MMP10. The model is based on the crystal structure of the catalytic domain of MMP10 (PDB 1q3a) (41) and the hexapeptide (PAE ↓ LVA) of the efficiently processed substrate peptide with E in P1. The glutamyl-leucine dipeptide harboring the scissile bond is shown. Catalytic Zn^{2+} ion is depicted in purple, and dashed lines indicate potential hydrogen-bond formation.

PAE ↓ LVA and performed docking experiments based on the crystal structure of the catalytic domain of MMP10 (PDB 1q3a) (41). After flexible ligand docking of the peptide to the active site cleft, we found potential interactions of the glutamate carboxyl side chain via hydrogen-bond formation with His^{182} and Ser^{179} of the S1 pocket (Fig. 3*B*). These potential interactions might induce a more efficient cleavage of substrates with E in P1.

MMP10-dependent Cleavage of Cell Adhesion Proteins and Secreted Bioactive Mediators—In addition to ECM substrates our dataset of newly identified MMP10-dependent processing events revealed cleavages in ectodomains of several cell adhesion proteins (Table I). These proteins contribute to adhesion complexes, which tether keratinocytes to the basement membrane and adjacent cells and are remodeled during cell migration at the wound edge (44). Among them and within subcluster M we identified the murine integrin alpha 6 subunit (ITGA6) by a neo-N-terminal peptide starting at position 518 within the extracellular domain (Fig. 4*A*). For validation of its direct processing by MMP10, we incubated recombinant human integrin alpha 6 beta 4, the functional heterodimer found at the basement membrane in the skin, with recombinant MMP10 and analyzed the mixtures by silver staining and immunoblot analysis. Thereby, silver staining revealed MMP10-generated cleavage products, one of which was also detected by a specific antibody for ITGA6, confirming a direct cleavage of ITGA6 by MMP10.

Of particular interest are MMP10-dependent cleavages in secreted bioactive mediators (Table I) whose processing might alter their activities as receptor ligands. Within subcluster M of MMP10-dependent cleavage events we identified dermokine (DMKN), a member of the stratified epithelium secreted peptides complex (45), by a neo-N terminus corresponding to a cleavage site after position 179 C-terminal to a collagen-like domain (COL) (Fig. 4*B*). To test for direct processing by MMP10, we incubated recombinant human DMKN with recombinant MMP10, which led to almost complete processing of full-length human DMKN (~50 kDa) and generation of cleavage products that were visualized by silver staining and immunoblot analysis and therefore confirmed direct processing of DMKN by MMP10.

Furthermore, as an MMP10-dependent cleavage event that was assigned to the subcluster of less efficient cleavages (subcluster S), we detected the extracellular protein cysteine-rich angiogenic inducer 61 (CYR61; also known as CCN1 and IGFBP10) by a neo-N terminus corresponding to a cleavage after position 137 within the von Willebrand factor type C domain (VWFC) (Fig. 4*C*). Immunoblot analysis of MMP10-incubated secretomes showed the presence of a cleavage product matching the expected molecular weight of ~12 kDa. Moreover, a cleavage fragment of the same size was also detected by immunoblot analysis of recombinant human CYR61 that was incubated with recombinant MMP10, thus validating CYR61 as a direct substrate for MMP10.

Finally, our iTRAQ-TAILS analysis identified MMP10-dependent processing of phosphatidylethanolamine-binding protein 1 (PEBP1) after position 13 that would lead to release of an N-terminal peptide also known as hippocampal cholinergic neurostimulating peptide (HCNP) (46). However, we failed to validate direct cleavage upon incubation of recombinant PEBP1 with active MMP10 (Fig. 4*D*). Therefore, based on the typical GPXX.L cleavage motif and because the same site had been identified for MMP2 (47), we tested for processing by MMP2 and MMP9 that either almost degraded (MMP2) or specifically cleaved (MMP9) PEBP1 *in vitro*. Moreover, gelatin zymography indicated presence and MMP10-dependent zymogen activation of MMP9 in keratinocyte secretomes (supplemental Fig. S1*A*) as well as direct activating processing of proMMP9 by MMP10 (supplemental Fig. S1*B*). This suggests an MMP10-MMP9 activation axis in keratinocytes that leads to processing of PEBP1.

Proteolytic Processing of DMKN in the Epidermis of K14-MMP10 Mice—In a next step and to validate and extend

TABLE I
MMP10-dependent processing of secreted and transmembrane proteins

Accession	Protein Name	Cleavage Site	Subcluster
Extracellular matrix processing			
Q05793	Basement membrane-specific heparan sulfate proteoglycan core protein (Perlecan;HSPG2)	AAAN^{2141}.^{2142}VHIP	M
P37889	Fibulin-2 (FBLN2)	CAAG^{921}.^{922}FLLA	M
Ectodomain shedding			
P55850	Desmocollin-3 (DSC3)	PFQF^{611}.^{612}NLAN	S
Q61739	Integrin alpha 6 (ITGA6)	PPIS^{517}.^{518}ILGI	M
O35988	Syndecan-4 (SDC4)	RPFP^{77}.^{78}EVIE	S
Cleavage of receptor ligands			
P18406	Cysteine-rich angiogenic inducer 61(CYR61)	CPQE^{137}.^{138}LSLP	S
Q6P253	Dermokine (DMKN)	GPLD^{179}.^{180}YETN	M
P04768	Proliferin-3 (PR2C3)	NPAW^{179}.^{180}FLQS	S
Q61207	Prosaposin (PSAP)	VVAP^{169}.^{170}FMSN	M
		SAYK^{520}.^{521}LLLG	M
Other			
P70296	Phosphatidylethanolamine-binding protein 1 (PEBP1)	GPLC^{13}.^{14}LQEV	M
Q9R118	Serine protease 11 (HTRA1)	APAA^{34}.^{35}TVCP	S
O70456	Stratifin (1433S)	MAAF^{25}.^{26}MKSA	S

findings from our cell-based studies, we analyzed MMP10-dependent cleavages *in vivo*. Because our current technologies do not yet allow the direct analysis of the very low amount of protein that can be obtained from wound epidermis, we prepared lysates from normal epidermis of mice expressing a constitutively active MMP10 mutant in basal keratinocytes (K14-MMP10) (7) ($n = 2$) and compared them to lysates from wild-type littermates ($n = 2$) by 4plex-iTRAQ-TAILS analysis (Fig. 5*A*). Combining data from analysis before and after TAILS N-terminal enrichment, we identified a total of 2079 proteins (supplemental Tables S4 and S5). These corresponded to 2900 N-terminal peptides (supplemental Table S5), of which according to UniProt/SwissProt annotation (available for 2150 N termini) 24% represented known mature protein N termini that were either blocked (acetylation, cyclization) (53%) or free (47%) and distributed to subcategories (initiator Met intact/removed; signal-/pro-/mitochrondrial transit-peptide removed) in ratios very similar to a previous analysis of total skin (Fig. 5*B*) (22). Around three quarters (76%) of N termini could not be assigned to known mature protein N termini and thus were derived from proteolytic cleavage, whereby 26% resulted from aminopeptidase activity, a common phenomenon, *e.g.* for processing of linker regions during maturation of structural skin proteins such as filaggrin (22, 48). From the remaining 50% we extracted 1173 N-terminally iTRAQ-labeled neo-N-terminal peptides representing true epidermal cleavages. These included only four of all 69 MMP10-dependent processing events identified in keratinocyte secretomes, but among them both collagen-like cleavages in DMKN and PEBP1 (Fig. 5*C*). Higher levels of MMP10 in the epidermis did not significantly alter abundances on the protein level (supplemental Fig. S2), but by quantitative analysis of epidermal cleavages we identified nine protein neo-N termini whose abundances were significantly ($p < 0.01$) and at least 1.4-fold ($\log_2$(K14-MMP10/wild-type) = 0.5) affected by MMP10 (Fig. 5*C*; supplemental Table S6). Strikingly, the only neo-N-terminal peptide with a significantly higher abundance in samples from MMP10 transgenic animals compared with wild-type controls was again the same DMKN peptide that we had also identified in our cell-based screen for MMP10 substrates (Fig. 5*D*). Hence, MMP10-dependent proteolytic processing of DMKN could be demonstrated both *in vitro* and *in vivo*.

DISCUSSION

In this study, we employed iTRAQ-TAILS on *in vitro* and *in vivo* samples to identify substrates of MMP10 that is highly expressed in migrating/invasively growing keratinocytes of skin wounds and cancers (4–6). Systematic substrate mining refined the MMP10 cleavage specificity and identified bioactive proteins as novel direct MMP10 targets that have been associated with cell adhesion, migration, proliferation and differentiation (Fig. 6) (49–51). MMP10-dependent but indirect cleavage of PEBP1 revealed a potential MMP10-MMP9 activation axis in keratinocyte secretomes, strengthening the hypothesis that MMP10 acts as a local activator within an interconnected MMP activation network (25, 52).

Because MMPs have not only disease promoting but also inhibiting functions (53, 54), a major challenge in current MMP inhibitor design is selectivity toward target MMPs (55, 56). Our refined specificity profile discriminates MMP10 *e.g.* from MMP2 and MMP9 that did not show a preference for an acidic amino acid in the P1 position in high-throughput profiling assays (23, 24, 47, 57). Interestingly, a glutamate in P1 was

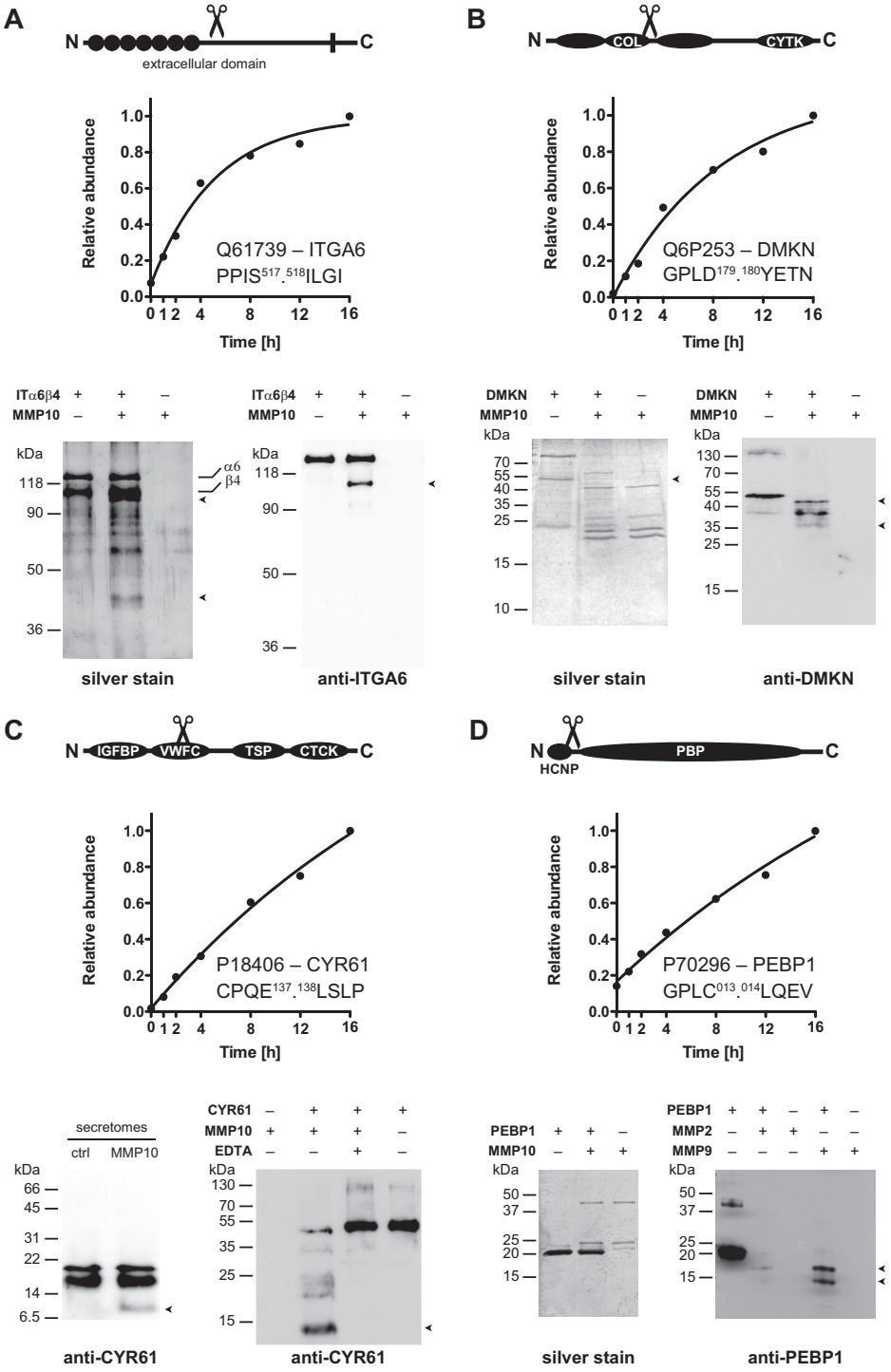

FIG. 4. **Validation of MMP10-dependent cleavage of ITGA6, DMKN, CYR61, and PEBP1.** Domain structures with annotated cleavage sites, time-dependent abundance profiles of generated neo-N termini and biochemical validation results are shown. *A*, Silver staining and immunoblot analysis of MMP10-incubated recombinant human integrin alpha 6 beta 4 (ITα6β4) revealed cleavage products with expected molecular weights and identified ITGA6 as a direct MMP10 substrate. *B*, Disappearance of the full-length protein and appearance of lower molecular weight fragments upon incubation of recombinant DMKN with MMP10 detected by silver staining and immunoblot indicated direct processing. COL: collagen-like domain; CTCK: cytokine-like domain. *C*, Detection of MMP10-generated fragments by immunoblot analysis of MMP10-treated keratinocyte secretomes and recombinant CYR61 confirmed direct processing by MMP10. IGFBP: insulin-like growth factor binding protein domain; TSP: thrombospondin domain; CTCK: C-terminal cystine knot domain. *D*, Lack of processing of recombinant PEBP1 by MMP10 (silver staining) indicated indirect cleavage in keratinocyte secretomes. Immunoblot analysis confirmed direct cleavage of the recombinant protein by MMP2 and MMP9.

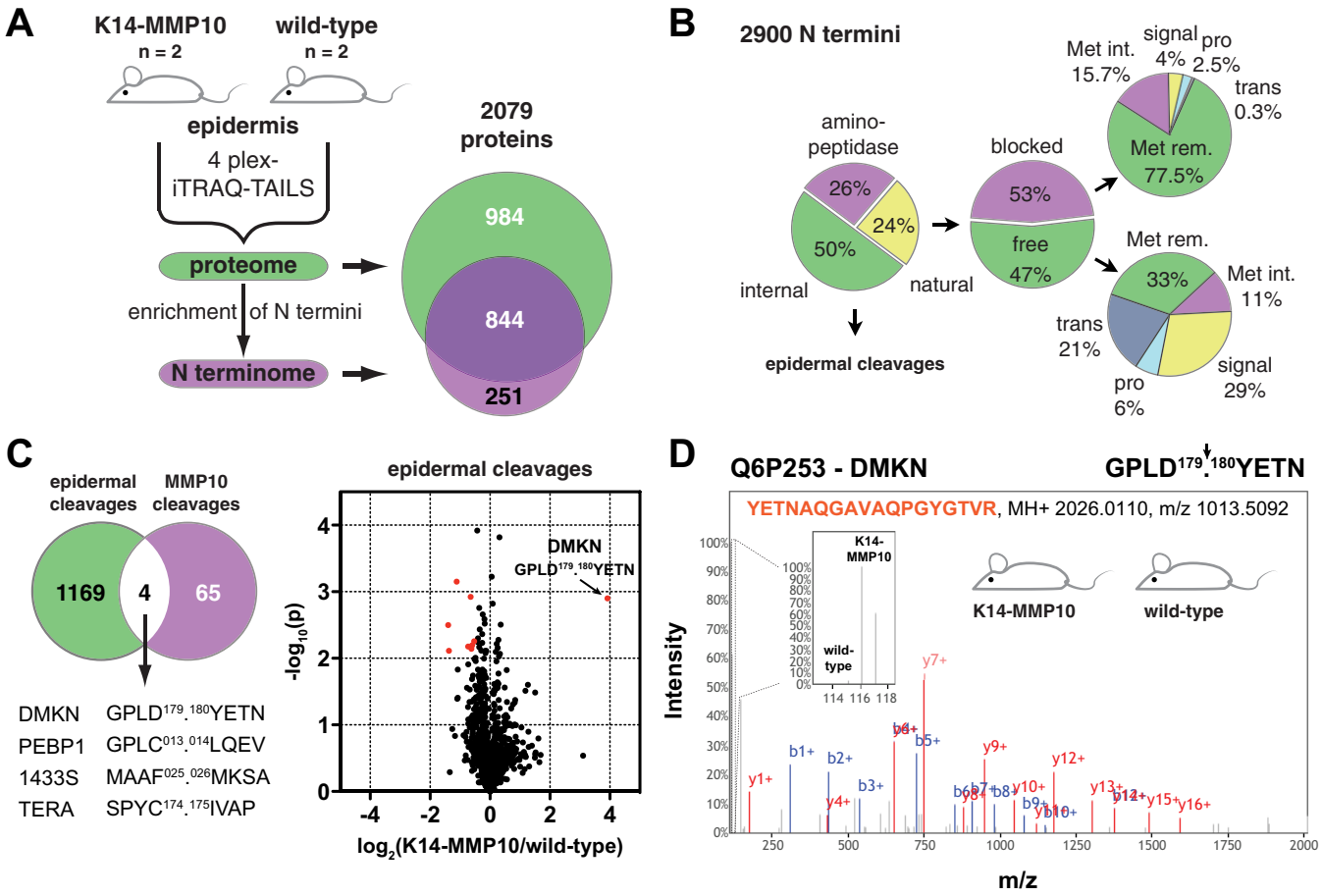

FIG. 5. **Degradomics analysis of epidermal lysates and validation of DMKN processing by MMP10 *in vivo*.** *A*, 4plex-iTRAQ-TAILS analysis of epidermal lysates from K14-MMP10 and wild-type mice (7). TAILS identified a total of 2079 proteins, of which 984 could be detected only by internal, 251 only by N-terminal and 844 by both types of peptides. *B*, Categorization of epidermal N termini according to UniProt/SwissProt annotation. A high proportion of N-terminal peptides were derived from aminopeptidase activity or endoproteolytic processing (epidermal cleavages). Natural mature protein N termini were either blocked (acetylation, cyclization) or free (iTRAQ-labeled) and subclassified (initiator Met int(act)/rem(oved); signal-/pro-/(mitochondrial) trans(it)-peptide removed) with similar proportions as described for total skin (22). *C*, *In vivo* analysis of MMP10-dependent proteolysis. Four out of 69 MMP10-related neo-N termini in keratinocyte secretomes were detected among 1173 epidermal cleavages (1433S: stratifin; TERA: transitional endoplasmic reticulum ATPase). Statistical analysis of differential abundance in samples from K14-MMP10 and wild-type mice (volcano plot) identified the MMP10-generated DMKN neo-N terminus as highly enriched in epidermis exposed to elevated MMP10 activity (one-sample *t* test on $\log_2$-ratios of replicate comparisons; red dots indicate neo-N termini with $p < 0.01$ and a fold change of at least 1.4 ($\log_2$(K14-MMP10/wild-type) = 0.5). *D*, Spectrum of the MMP10-dependent neo-N-terminal peptide derived from DMKN in epidermal lysates from K14-MMP10 mice and wild-type littermates. iTRAQ reporter ions indicate high abundance of the peptide only in samples from transgenic animals.

also instrumental in developing a peptide substrate with selectivity for MMP3 (58), which shares 78% overall amino acid identity with MMP10 and shows no significant structural differences in the catalytic domain (41). Notably, Ser^{179} that our docking analysis identified as a potential hydrogen bonding partner for P1 glutamate residues is compared with other MMPs unique for MMP10 in this position (59). More in-depth analyses are needed, but this newly identified preference might be exploited for the development of more specific activity-based probes and inhibitors targeting MMP10 in cancer.

ITGA6 forms dimers with the integrin beta 4 subunit (ITGB4) to mediate adhesion of basal keratinocytes to the basement membrane via binding to laminin-332 in adhesive complexes termed hemidesmosomes (60). Upon injury, hemidesmosomes have to be disassembled at the leading wound edge to facilitate migration of keratinocytes along the injured dermis and the newly formed provisional matrix (60, 61). Recent results suggest that clipping off these adhesive structures by limited proteolysis might contribute to this process in wound healing as well as during carcinogenesis (62, 63). Thereby, MMP9 can cleave ITGB4 (62), and our new data suggest that it may act synergistically with MMP10 upon local activation. Hence, together with desmocollin-3, syndecan-4 (SDC4), perlecan, fibulin-2 and laminin-332 as substrates, our data support the hypothesis that MMP10 is involved in the control of keratinocyte migration by breakdown of adhesion com-

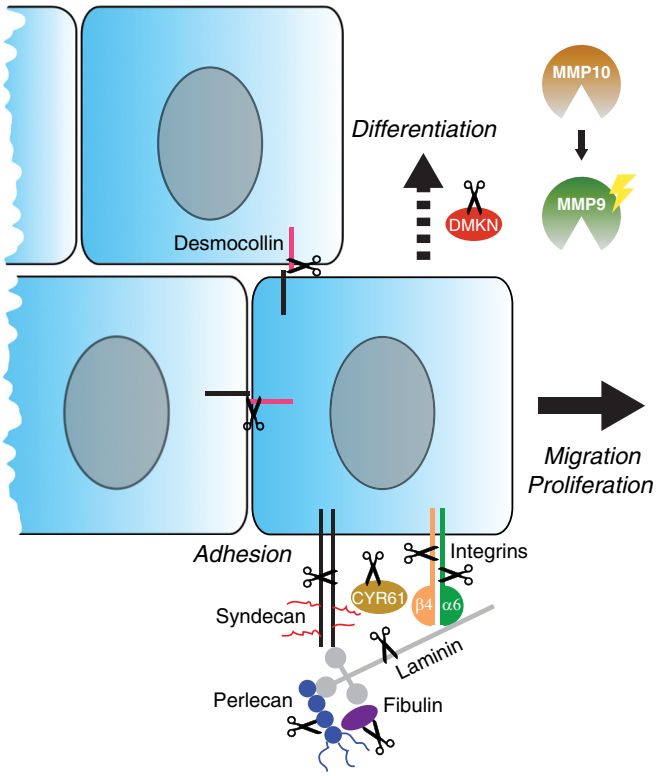

FIG. 6. **Integrated hypothetical model of MMP10 activities at the wound edge.** MMP10 cleaves multiple components of hemidesmosomes (laminin-332, integrin alpha 6, perlecan, fibulin-2), desmosomes (desmocollin-3), and associated cell adhesion molecules (syndecan-4) to contribute to release of proliferating and migrating keratinocytes at the wound margin. Furthermore, MMP10 processes soluble bioactive mediators (dermokine (DMKN), CYR61) to modulate their activities in control of keratinocyte proliferation, migration (CYR61) and differentiation (DMKN). Finally, MMP10 activates proMMP9 that complements MMP10 functions and processes additional substrates.

plexes, followed by degradation of basement membrane and matrix components (7).

In cutaneous wounds, expression of CYR61 is strongly induced in the granulation tissue, where it stimulates angiogenesis and restricts fibrosis by induction of fibroblast senescence (64, 65). However, high levels of CYR61 have also been reported in keratinocytes and are associated with epidermal hyperplasia in psoriatic lesions and basal cell carcinoma (66–68). Although specific receptors for these activities in keratinocytes remain to be identified, CYR61 acts on endothelial cells and fibroblasts by selective binding of motifs in individual N- and C-terminal domains to distinct integrin heterodimers and heparin sulfate proteoglycans, including ITGA6 and SDC4 (65, 69). A central hinge domain is susceptible to cleavage *e.g.* by kallikrein-7 (70) whose activity in keratinocyte secretomes might explain the appearance of smaller molecular weight fragments, of which the N-terminal part is further processed by MMP10 (Fig. 5*C*). Interestingly, MMP10 released fragments of the same sizes from recombinant CYR61 as MMP14 (71). The latter is expressed by stromal cells upon wounding (72) and might modulate CYR61 activities in the granulation tissue, whereas our results suggest that MMP10 leads to similar cleavages in the epidermis.

MMP10-dependent processing of DMKN is of particular interest, because DMKN expression in skin wounds spatially and temporally overlaps with increased levels of MMP10 in wound edge keratinocytes (4, 73–75). Moreover, recombinant DMKN inhibited ERK phosphorylation in cultured keratinocytes and delayed wound closure in mice (75, 76). However, the mechanisms of DMKN activity in keratinocyte differentiation and inflammatory skin diseases remain to be determined. We propose that proteolytic processing provides an additional level of regulation for this potential soluble mediator. Indeed, processing of DMKN by cathepsin B in the skin has recently been reported (77). Notably, cleavage of DMKN by MMP10 did not obviously impact epidermal differentiation in the skin of K14-MMP10 mice (7). Thus, it will be important to analyze the consequences of MMP10-mediated proteolytic modification of DMKN in a hyperproliferative epidermis, where keratinocytes acquire an activated state with altered differentiation (78).

PEBP1, also known as Raf Kinase inhibitory protein (RKIP), is as a cytoplasmic protein that regulates intracellular kinase signaling in responses to multiple stimuli (46). However, PEBP1 can be also released into the extracellular environment by alternative secretion and act as a soluble factor (79). These functions are mediated by an N-terminal peptide, which is proteolytically removed from PEBP1 and that was named hippocampal cholinergic neurostimulating peptide (HCNP) because of its functions in neuronal differentiation and acetylcholine synthesis (80). HCNP also acts as an endocrine factor in cardiac physiology, demonstrating a role in nonneuronal organs (79, 81). MMP10-dependent cleavage of PEBP1 after Cys^{13} generates a peptide that only differs by an additional C-terminal cysteine from HCNP and thus can most likely exert the same functions. This would provide a mechanism to release HCNP from secreted PEBP1 in addition to cleavage by a yet unspecified cysteine protease (82), which might process the protein within secretory granules. Importantly, PEBP1 was also identified in secretomes from human primary keratinocytes (83), and cleavage at the same site was detected in fibroblast supernatants upon incubation with MMP2 (47) as well as *in vivo* in murine skin lysates (22). Finally, MMP10-dependent but indirect processing, which is most likely mediated by activated MMP9 further supports the concept of MMP10 as an activating protease that locally controls activity of other MMPs at the wound margin (52). This indirect activity might also explain the lack of significant differences in abundance of the PEBP1 neo-N terminus in epidermal lysates from K14-MMP10 and wild-type animals, because only minimal levels of MMP9 are present in normal skin (84). Together, these findings warrant further studies on the potential roles of PEBP1 and HCNP in the skin and upon injury.

With more than 2000 proteins and almost 3000 N termini we recorded the most comprehensive epidermal proteome and N-terminome reported to date and specifically increased coverage of the epidermis compared with previous studies that analyzed lysates from whole skin (22, 77). The only very minor quantitative effects of increased abundance of MMP10 on proteins in the epidermis could be attributed to expression of the transgene in only a small fraction of the cells contributing to the epidermal lysates, but they also reflect the robustness of the proteolytic network in the skin that was also not dramatically affected by loss of individual cathepsins or MMP2 under unchallenged conditions (22, 77). Moreover, because of the significantly higher complexity of the sample, TAILS presumably missed many substrate cleavages in epidermal lysates that had been identified in the cell-based screen. This is in agreement with previous studies, which analyzed cathepsins or MMPs using *in vitro* and *in vivo* systems (22, 47, 77, 85). Finally, many substrates might only be accessible to MMP10-dependent processing at the very tip of the wound epidermis or the invasive front of tumors, when keratinocytes are exposed to proliferative and migratory stimuli and an altered extracellular environment (78, 86). Thus, more sensitive technologies are needed to precisely monitor locally restricted protease activity in defined tissue compartments.

In summary, using advanced mass spectrometry-based degradomics we assessed the MMP10 substrate degradome in the epidermis *in vitro* and *in vivo* and generated new testable hypotheses for further exploration of this disease-related protease and its contribution to interconnected MMP activities that modulate keratinocyte behavior at the edge of hyperproliferative epithelia. Our findings pave the way for future studies that are needed to determine, if and to what extend the newly identified substrate cleavages indeed determine MMP10 function in skin repair and carcinogenesis.

Acknowledgments—We thank Sabine Werner (ETH Zurich) for continuous support, very helpful suggestions, and discussions. A special thanks goes to the proteomics team from the Functional Genomics Center Zurich (FGCZ) for excellent support in mass spectrometry. We thank Fabian Egli (ETH Zurich) for generation of secondary structure logos, Grace Tang (ETH Zurich) for help with immunoblot analysis and Chris Overall (UBC Vancouver) for kindly providing recombinant MMP9.

* This work was supported by grants from the Swiss National Science Foundation (31003A_140726) and from the European Commission (Marie Curie International Reintegration Grant; FP7-PEOPLE-2010-RG/SkiNterminomics) to U.a.d.K. and by funds from the ETH Zurich. F.S. is supported by a predoctoral fellowship from the Portuguese Foundation for Science and Technology (FCT) (SFRH/BD/88564/2012). J.N.K. acknowledges a Michael Smith Foundation for Health Research Career Investigator Scholar Award. We declare no competing financial interest.

S This article contains supplemental Figs. S1, S2 and Tables S1 to S6.

¶ To whom correspondence should be addressed: ETH Zurich, Otto-Stern-Weg 7 HPL, F14.2, Zurich 8093 Switzerland. Tel.: 41-44-633 3392; Fax: +41-44-633-1147; E-mail: ulrich.aufdemkeller@biol.ethz.ch.

REFERENCES

1. Toriseva, M., and Kähäri, V. M. (2009) Proteinases in cutaneous wound healing. *Cell. Mol. Life Sci.* **66,** 203–224
2. Egeblad, M., and Werb, Z. (2002) New functions for the matrix metalloproteinases in cancer progression. *Nat. Rev. Cancer* **2,** 161–174
3. Sabino, F., and auf dem Keller, U. (2015) Matrix metalloproteinases in impaired wound healing. *Metalloproteinases Med.* **2,** 1–8
4. Madlener, M., Mauch, C., Conca, W., Brauchle, M., Parks, W. C., and Werner, S. (1996) Regulation of the expression of stromelysin-2 by growth factors in keratinocytes: implications for normal and impaired wound healing. *Biochem. J.* **320**, 659–664
5. Saarialho-Kere, U. K., Pentland, A. P., Birkedal-Hansen, H., Parks, W. C., and Welgus, H. G. (1994) Distinct populations of basal keratinocytes express stromelysin-1 and stromelysin-2 in chronic wounds. *J. Clin. Invest.* **94,** 79–88
6. Kerkelä, E., Ala-aho, R., Lohi, J., Grénman, R., M-Kähäri, V., and Saarialho-Kere, U. (2001) Differential patterns of stromelysin-2 (MMP-10) and MT1-MMP (MMP-14) expression in epithelial skin cancers. *Br. J. Cancer* **84,** 659–669
7. Krampert, M., Bloch, W., Sasaki, T., Bugnon, P., Kerkelä, T., Wolf, E., Aumailley, M., Parks, W. C., and Werner, S. (2004) Activities of the matrix metalloproteinase stromelysin-2 (MMP-10) in matrix degradation and keratinocyte organization in wounded skin. *Mol. Biol. Cell* **15,** 5242–5254
8. Kassim, S. Y., Gharib, S. A., Mecham, B. H., Birkland, T. P., Parks, W. C., and McGuire, J. K. (2007) Individual matrix metalloproteinases control distinct transcriptional responses in airway epithelial cells infected with Pseudomonas aeruginosa. *Infect. Immun.* **75,** 5640–5650
9. Koller, F. L., Dozier, E. A., Nam, K. T., Swee, M., Birkland, T. P., Parks, W. C., and Fingleton, B. (2012) Lack of MMP10 exacerbates experimental colitis and promotes development of inflammation-associated colonic dysplasia. *Lab. Invest.* **92,** 1749–1759
10. Garcia-Irigoyen, O., Carotti, S., Latasa, M. U., Uriarte, I., Fernández -Barrena, M. G., Elizalde, M., Urtasun, R., Vespasiani-Gentilucci, U., Morini, S., Banales, J. M., Parks, W. C., Rodriguez, J. A., Orbe, J., Prieto, J., Páramo, J. A., Berasain, C., and Ávila, M. A. (2014) Matrix metalloproteinase-10 expression is induced during hepatic injury and plays a fundamental role in liver tissue repair. *Liver Int.* **34,** e257–270
11. García -Irigoyen, O., Latasa, M. U., Carotti, S., Uriarte, I., Elizalde, M., Urtasun, R., Vespasiani-Gentilucci, U., Morini, S., Benito, P., Ladero, J. M., Rodriguez, J. A., Prieto, J., Orbe, J., Páramo, J. A., Fernández -Barrena, M. G., Berasain, C., and Avila, M. A. (2015) Matrix metalloproteinase 10 contributes to hepatocarcinogenesis in a novel crosstalk with the stromal derived factor 1/C-X-C chemokine receptor 4 axis. *Hepatology* **62,** 166–178
12. Rohani, M. G., McMahan, R. S., Razumova, M. V., Hertz, A. L., Cieslewicz, M., Pun, S. H., Regnier, M., Wang, Y., Birkland, T. P., and Parks, W. C. (2015) MMP-10 Regulates Collagenolytic Activity of Alternatively Activated Resident Macrophages. *J. Invest. Dermatol.* **135,** 2377–2384
13. Nagase, H., and Woessner, J. F., Jr. (1999) Matrix metalloproteinases. *J. Biol. Chem.* **274,** 21491–21494
14. Van Lint, P., and Libert, C. (2007) Chemokine and cytokine processing by matrix metalloproteinases and its effect on leukocyte migration and inflammation. *J. Leukoc. Biol.* **82,** 1375–1381
15. Rodríguez, D., Morrison, C. J., and Overall, C. M. (2010) Matrix metalloproteinases: what do they not do? New substrates and biological roles identified by murine models and proteomics. *Biochim. Biophys. Acta* **1803,** 39–54
16. Page-McCaw, A., Ewald, A. J., and Werb, Z. (2007) Matrix metalloproteinases and the regulation of tissue remodelling. *Nat. Rev. Mol. Cell Biol.* **8,** 221–233
17. McCawley, L. J., Wright, J., LaFleur, B. J., Crawford, H. C., and Matrisian, L. M. (2008) Keratinocyte expression of MMP3 enhances differentiation and prevents tumor establishment. *Am. J. Pathol.* **173,** 1528–1539
18. Noë, V., Fingleton, B., Jacobs, K., Crawford, H. C., Vermeulen, S., Steelant, W., Bruyneel, E., Matrisian, L. M., and Mareel, M. (2001) Release of an invasion promoter E-cadherin fragment by matrilysin and stromelysin-1. *J. Cell Sci.* **114,** 111–118
19. McCawley, L. J., Crawford, H. C., King, L. E., Jr., Mudgett, J., and Matrisian, L. M. (2004) A protective role for matrix metalloproteinase-3 in

squamous cell carcinoma. *Cancer Res.* **64,** 6965–6972
20. McCawley, L. J., and Matrisian, L. M. (2001) Matrix metalloproteinases: they're not just for matrix anymore! *Curr. Opin. Cell Biol.* **13,** 534–540
21. Nagase, H. (2013) Chapter 158 - Matrix Metalloproteinase 3/Stromelysin 1. In: Salvesen, N. D. R., ed. *Handbook of Proteolytic Enzymes*, pp. 763–774, Academic Press
22. auf dem Keller, U., Prudova, A., Eckhard, U., Fingleton, B., and Overall, C. M. (2013) Systems-level analysis of proteolytic events in increased vascular permeability and complement activation in skin inflammation. *Sci. Signal.* **6,** rs2
23. Kleifeld, O., Doucet, A., Prudova, A., auf dem Keller, U., Gioia, M., Kizhakkedathu, J. N., and Overall, C. M. (2011) Identifying and quantifying proteolytic events and the natural N terminome by terminal amine isotopic labeling of substrates. *Nat. Protoc.* **6,** 1578–1611
24. Prudova, A., auf dem Keller, U., Butler, G. S., and Overall, C. M. (2010) Multiplex N-terminome analysis of MMP-2 and MMP-9 substrate degradomes by iTRAQ-TAILS quantitative proteomics. *Mol. Cell. Proteomics* **9,** 894–911
25. Schlage, P., Egli, F. E., Nanni, P., Wang, L. W., Kizhakkedathu, J. N., Apte, S. S., and auf dem Keller, U. (2014) Time-resolved analysis of the matrix metalloproteinase 10 substrate degradome. *Mol. Cell. Proteomics* **13,** 580–593
26. Schlage, P., Kockmann, T., Kizhakkedathu, J. N., and auf dem Keller, U. (2015) Monitoring matrix metalloproteinase activity at the epidermal-dermal interface by SILAC-iTRAQ-TAILS. *Proteomics* **15,** 2491–2502
27. Durchdewald, M., Beyer, T. A., Johnson, D. A., Johnson, J. A., Werner, S., and auf dem Keller, U. (2007) Electrophilic chemicals but not UV irradiation or reactive oxygen species activate Nrf2 in keratinocytes in vitro and in vivo. *J. Invest. Dermatol.* **127,** 646–653
28. auf dem Keller, U., Huber, M., Beyer, T. A., Kümin, A., Siemes, C., Braun, S., Bugnon, P., Mitropoulos, V., Johnson, D. A., Johnson, J. A., Hohl, D., and Werner, S. (2006) Nrf transcription factors in keratinocytes are essential for skin tumor prevention but not for wound healing. *Mol. Cell. Biol.* **26,** 3773–3784
29. Kleifeld, O., Doucet, A., auf dem Keller, U., Prudova, A., Schilling, O., Kainthan, R. K., Starr, A. E., Foster, L. J., Kizhakkedathu, J. N., and Overall, C. M. (2010) Isotopic labeling of terminal amines in complex samples identifies protein N-termini and protease cleavage products. *Nat. Biotechnol.* **28,** 281–288
30. Deutsch, E. W., Mendoza, L., Shteynberg, D., Farrah, T., Lam, H., Tasman, N., Sun, Z., Nilsson, E., Pratt, B., Prazen, B., Eng, J. K., Martin, D. B., Nesvizhskii, A. I., and Aebersold, R. (2010) A guided tour of the Trans-Proteomic Pipeline. *Proteomics* **10,** 1150–1159
31. Shadforth, I. P., Dunkley, T. P., Lilley, K. S., and Bessant, C. (2005) i-Tracker: for quantitative proteomics using iTRAQ. *BMC Genomics* **6,** 145
32. auf dem Keller, U., and Overall, C. M. (2012) CLIPPER-An add-on to the Trans-Proteomic Pipeline for the automated analysis of TAILS N-terminomics data. *Biol. Chem.* **393,** 1477–1483
33. Kumar, L. E., and Futschik, M. (2007) Mfuzz: a software package for soft clustering of microarray data. *Bioinformation* **2,** 5–7
34. Schwämmle, V., and Jensen, O. N. (2010) A simple and fast method to determine the parameters for fuzzy c-means cluster analysis. *Bioinformatics* **26,** 2841–2848
35. Schilling, O., auf dem Keller, U., and Overall, C. M. (2011) Factor Xa subsite mapping by proteome-derived peptide libraries improved using WebPICS, a resource for proteomic identification of cleavage sites. *Biol. Chem.* **392,** 1031–1037
36. Colaert, N., Helsens, K., Martens, L., Vandekerckhove, J., and Gevaert, K. (2009) Improved visualization of protein consensus sequences by iceLogo. *Nat. Methods* **6,** 786–787
37. Sabino, F., Hermes, O., Egli, F. E., Kockmann, T., Schlage, P., Croizat, P., Kizhakkedathu, J. N., Smola, H., and auf dem Keller, U. (2015) In vivo assessment of protease dynamics in cutaneous wound healing by degradomics analysis of porcine wound exudates. *Mol. Cell. Proteomics* **14,** 354–370
38. Saeed, A. I., Sharov, V., White, J., Li, J., Liang, W., Bhagabati, N., Braisted, J., Klapa, M., Currier, T., Thiagarajan, M., Sturn, A., Snuffin, M., Rezantsev, A., Popov, D., Ryltsov, A., Kostukovich, E., Borisovsky, I., Liu, Z., Vinsavich, A., Trush, V., and Quackenbush, J. (2003) TM4: a free, open-source system for microarray data management and analysis. *BioTechniques* **34,** 374–378
39. Jones, D. T. (1999) Protein secondary structure prediction based on position-specific scoring matrices. *J. Mol. Biol.* **292,** 195–202
40. Crooks, G. E., Hon, G., Chandonia, J. M., and Brenner, S. E. (2004) WebLogo: a sequence logo generator. *Genome Res.* **14,** 1188–1190
41. Bertini, I., Calderone, V., Fragai, M., Luchinat, C., Mangani, S., and Terni, B. (2004) Crystal structure of the catalytic domain of human matrix metalloproteinase 10. *J. Mol. Biol.* **336,** 707–716
42. Coleman, R. G., Carchia, M., Sterling, T., Irwin, J. J., and Shoichet, B. K. (2013) Ligand pose and orientational sampling in molecular docking. *PLoS ONE* **8,** e75992
43. Vizcaíno, J. A., Deutsch, E. W., Wang, R., Csordas, A., Reisinger, F., Rios, D., Dianes, J. A., Sun, Z., Farrah, T., Bandeira, N., Binz, P. A., Xenarios, I., Eisenacher, M., Mayer, G., Gatto, L., Campos, A., Chalkley, R. J., Kraus, H. J., Albar, J. P., Martinez-Bartolome, S., Apweiler, R., Omenn, G. S., Martens, L., Jones, A. R., and Hermjakob, H. (2014) ProteomeXchange provides globally coordinated proteomics data submission and dissemination. *Nat. Biotechnol.* **32,** 223–226
44. Hopkinson, S. B., Hamill, K. J., Wu, Y., Eisenberg, J. L., Hiroyasu, S., and Jones, J. C. (2014) Focal contact and hemidesmosomal proteins in keratinocyte migration and wound repair. *Adv. Wound Care* **3,** 247–263
45. Matsui, T., Hayashi-Kisumi, F., Kinoshita, Y., Katahira, S., Morita, K., Miyachi, Y., Ono, Y., Imai, T., Tanigawa, Y., Komiya, T., and Tsukita, S. (2004) Identification of novel keratinocyte-secreted peptides dermokine-alpha/-beta and a new stratified epithelium-secreted protein gene complex on human chromosome 19q13.1. *Genomics* **84,** 384–397
46. Al-Mulla, F., Bitar, M. S., Taqi, Z., and Yeung, K. C. (2013) RKIP: much more than Raf kinase inhibitory protein. *J. Cell. Physiol.* **228,** 1688–1702
47. auf dem Keller, U., Prudova, A., Gioia, M., Butler, G. S., and Overall, C. M. (2010) A statistics-based platform for quantitative N-terminome analysis and identification of protease cleavage products. *Mol. Cell. Proteomics* **9,** 912–927
48. Resing, K. A., Johnson, R. S., and Walsh, K. A. (1993) Characterization of protease processing sites during conversion of rat profilaggrin to filaggrin. *Biochemistry* **32,** 10036–10045
49. Naso, M. F., Liang, B., Huang, C. C., Song, X. Y., Shahied-Arruda, L., Belkowski, S. M., D'Andrea, M. R., Polkovitch, D. A., Lawrence, D. R., Griswold, D. E., Sweet, R. W., and Amegadzie, B. Y. (2007) Dermokine: an extensively differentially spliced gene expressed in epithelial cells. *J. Invest. Dermatol.* **127,** 1622–1631
50. Sonnenberg, A., Calafat, J., Janssen, H., Daams, H., van der Raaij-Helmer, L. M., Falcioni, R., Kennel, S. J., Aplin, J. D., Baker, J., Loizidou, M., and et al. (1991) Integrin alpha 6/beta 4 complex is located in hemidesmosomes, suggesting a major role in epidermal cell-basement membrane adhesion. *J. Cell Biol.* **113,** 907–917
51. Jun, J. I., and Lau, L. F. (2011) Taking aim at the extracellular matrix: CCN proteins as emerging therapeutic targets. *Nat. Rev. Drug Discov.* **10,** 945–963
52. Nakamura, H., Fujii, Y., Ohuchi, E., Yamamoto, E., and Okada, Y. (1998) Activation of the precursor of human stromelysin 2 and its interactions with other matrix metalloproteinases. *Eur. J. Biochem.* **253,** 67–75
53. Overall, C. M., and Kleifeld, O. (2006) Tumour microenvironment - opinion: validating matrix metalloproteinases as drug targets and anti-targets for cancer therapy. *Nat. Rev. Cancer* **6,** 227–239
54. López-Otín, C., and Matrisian, L. M. (2007) Emerging roles of proteases in tumour suppression. *Nat. Rev. Cancer* **7,** 800–808
55. Devel, L., Czarny, B., Beau, F., Georgiadis, D., Stura, E., and Dive, V. (2010) Third generation of matrix metalloprotease inhibitors: Gain in selectivity by targeting the depth of the S1′ cavity. *Biochimie* **2,** 1501–1508
56. Pirard, B. (2007) Insight into the structural determinants for selective inhibition of matrix metalloproteinases. *Drug Discov. Today* **12,** 640–646
57. Schilling, O., and Overall, C. M. (2008) Proteome-derived, database-searchable peptide libraries for identifying protease cleavage sites. *Nat. Biotechnol.* **26,** 685–694
58. Nagase, H., Fields, C. G., and Fields, G. B. (1994) Design and characterization of a fluorogenic substrate selectively hydrolyzed by stromelysin 1 (matrix metalloproteinase-3). *J. Biol. Chem.* **269,** 20952–20957
59. Maskos, K. (2005) Crystal structures of MMPs in complex with physiological and pharmacological inhibitors. *Biochimie* **87,** 249–263
60. Margadant, C., Charafeddine, R. A., and Sonnenberg, A. (2010) Unique and redundant functions of integrins in the epidermis. *FASEB J.* **24,** 4133–4152

61. Green, K. J., Getsios, S., Troyanovsky, S., and Godsel, L. M. (2010) Intercellular junction assembly, dynamics, and homeostasis. *Cold Spring Harb. Perspect. Biol.* 2:a000125
62. Pal-Ghosh, S., Blanco, T., Tadvalkar, G., Pajoohesh-Ganji, A., Parthasarathy, A., Zieske, J. D., and Stepp, M. A. (2011) MMP9 cleavage of the β4 integrin ectodomain leads to recurrent epithelial erosions in mice. *J. Cell Sci.* **124,** 2666–2675
63. Pawar, S. C., Demetriou, M. C., Nagle, R. B., Bowden, G. T., and Cress, A. E. (2007) Integrin alpha6 cleavage: a novel modification to modulate cell migration. *Exp. Cell Res.* **313,** 1080–1089
64. Jun, J. I., and Lau, L. F. (2010) The matricellular protein CCN1 induces fibroblast senescence and restricts fibrosis in cutaneous wound healing. *Nat. Cell Biol.* **12,** 676–685
65. Lau, L. F. (2011) CCN1/CYR61: the very model of a modern matricellular protein. *Cell. Mol. Life Sci.* **68,** 3149–3163
66. Sun, Y., Zhang, J., Zhou, Z., Wu, P., Huo, R., Wang, B., Shen, Z., Li, H., Zhai, T., Shen, B., Chen, X., and Li, N. (2015) CCN1, a Pro-Inflammatory Factor, Aggravates Psoriasis Skin Lesions by Promoting Keratinocyte Activation. *J. Invest. Dermatol.*, doi:10.1038/jid.2015.231
67. Quan, T., Xu, Y., Qin, Z., Robichaud, P., Betcher, S., Calderone, K., He, T., Johnson, T. M., Voorhees, J. J., and Fisher, G. J. (2014) Elevated YAP and its downstream targets CCN1 and CCN2 in basal cell carcinoma: impact on keratinocyte proliferation and stromal cell activation. *Am. J. Pathol.* **184,** 937–943
68. Zhang, H., Pasolli, H. A., and Fuchs, E. (2011) Yes-associated protein (YAP) transcriptional coactivator functions in balancing growth and differentiation in skin. *Proc. Natl. Acad. Sci. U.S.A.* **108,** 2270–2275
69. Holbourn, K. P., Acharya, K. R., and Perbal, B. (2008) The CCN family of proteins: structure-function relationships. *Trends Biochem. Sci.* **33,** 461–473
70. Yu, Y., Prassas, I., Dimitromanolakis, A., and Diamandis, E. P. (2015) Novel Biological Substrates of Human Kallikrein 7 Identified through Degradomics. *J. Biol. Chem.* **290,** 17762–17775
71. Butler, G. S., Dean, R. A., Tam, E. M., and Overall, C. M. (2008) Pharmacoproteomics of a metalloproteinase hydroxamate inhibitor in breast cancer cells: dynamics of membrane type 1 matrix metalloproteinase-mediated membrane protein shedding. *Mol. Cell. Biol.* **28,** 4896–4914
72. Okada, A., Tomasetto, C., Lutz, Y., Bellocq, J. P., Rio, M. C., and Basset, P. (1997) Expression of matrix metalloproteinases during rat skin wound healing: evidence that membrane type-1 matrix metalloproteinase is a stromal activator of pro-gelatinase A. *J. Cell Biol.* **137,** 67–77
73. Leclerc, E. A., Huchenq, A., Kezic, S., Serre, G., and Jonca, N. (2014) Mice deficient for the epidermal dermokine beta and gamma isoforms display transient cornification defects. *J. Cell Sci.* **127,** 2862–2872
74. Hasegawa, M., Higashi, K., Yokoyama, C., Yamamoto, F., Tachibana, T., Matsushita, T., Hamaguchi, Y., Saito, K., Fujimoto, M., and Takehara, K. (2013) Altered expression of dermokine in skin disorders. *J. Eur. Acad. Dermatol. Venereol.* **27,** 867–875
75. Hasegawa, M., Higashi, K., Matsushita, T., Hamaguchi, Y., Saito, K., Fujimoto, M., and Takehara, K. (2013) Dermokine inhibits ELR(+)CXC chemokine expression and delays early skin wound healing. *J. Dermatol. Sci.* **70,** 34–41
76. Higashi, K., Hasegawa, M., Yokoyama, C., Tachibana, T., Mitsui, S., and Saito, K. (2012) Dermokine-beta impairs ERK signaling through direct binding to GRP78. *FEBS Lett.* **586,** 2300–2305
77. Tholen, S., Biniossek, M. L., Gansz, M., Gomez-Auli, A., Bengsch, F., Noel, A., Kizhakkedathu, J. N., Boerries, M., Busch, H., Reinheckel, T., and Schilling, O. (2013) Deletion of cysteine cathepsins B or L yields differential impacts on murine skin proteome and degradome. *Mol. Cell. Proteomics* **12,** 611–625
78. Freedberg, I. M., Tomic-Canic, M., Komine, M., and Blumenberg, M. (2001) Keratins and the keratinocyte activation cycle. *J. Invest. Dermatol.* **116,** 633–640
79. Goumon, Y., Angelone, T., Schoentgen, F., Chasserot-Golaz, S., Almas, B., Fukami, M. M., Langley, K., Welters, I. D., Tota, B., Aunis, D., and Metz-Boutigue, M. H. (2004) The hippocampal cholinergic neurostimulating peptide, the N-terminal fragment of the secreted phosphatidylethanolamine-binding protein, possesses a new biological activity on cardiac physiology. *J. Biol. Chem.* **279,** 13054–13064
80. Ojika, K., Kojima, S., Ueki, Y., Fukushima, N., Hayashi, K., and Yamamoto, M. (1992) Purification and structural analysis of hippocampal cholinergic neurostimulating peptide. *Brain Res.* **572,** 164–171
81. Angelone, T., Goumon, Y., Cerra, M. C., Metz-Boutigue, M. H., Aunis, D., and Tota, B. (2006) The emerging cardioinhibitory role of the hippocampal cholinergic neurostimulating peptide. *J. Pharmacol. Exp. Ther.* **318,** 336–344
82. Otsuka, Y., and Ojika, K. (1996) Demonstration and characterization of hippocampal cholinergic neurostimulating peptide (HCNP) processing enzyme activity in rat hippocampus. *Neurochem. Res.* **21,** 369–376
83. Keller, M., Rüegg, A., Werner, S., and Beer, H.-D. (2008) Active caspase-1 is a regulator of unconventional protein secretion. *Cell* **132,** 818–831
84. Madlener, M., Parks, W. C., and Werner, S. (1998) Matrix metalloproteinases (MMPs) and their physiological inhibitors (TIMPs) are differentially expressed during excisional skin wound repair. *Exp. Cell Res.* **242,** 201–210
85. Tholen, S., Biniossek, M. L., Gessler, A. L., Müller, S., Weisser, J., Kizhakkedathu, J. N., Reinheckel, T., and Schilling, O. (2011) Contribution of cathepsin L to secretome composition and cleavage pattern of mouse embryonic fibroblasts. *Biol. Chem.* **392,** 961–971
86. Pastar, I., Stojadinovic, O., Yin, N. C., Ramirez, H., Nusbaum, A. G., Sawaya, A., Patel, S. B., Khalid, L., Isseroff, R. R., and Tomic-Canic, M. (2014) Epithelialization in Wound Healing: A Comprehensive Review. *Adv Wound Care* **3,** 445–464